ARCHAEOMETRIC ANALYSES OF TRANSYLVANIAN METAL ARTEFACTS. CASE STUDY: THE SCYTHIAN NECROPOLIS OF SÂNCRAI (ALBA COUNTY)

GABRIEL BALTEŞ, MIHAI GLIGOR, IOANA D. DULAMĂ,
CRISTIANA RĂDULESCU, SOFIA TEODORESCU, RALUCA M. ŞTIRBESCU,
IOAN A. BUCURICĂ, AND SORINA G. STĂNESCU*

Introduction

In recent decades, numerous archaeological discoveries have provided information concerning the historical past of the populations that settled in the Carpathian-Danubian-Pontic area during various historical periods. In this context, the investigation of the Sâncrai necropolis (Alba County) has played an important role in building knowledge regarding the Scythian horizon in Transylvania. Most of the discoveries concerning this group or groups of Eurasian people were made in the middle basin of the Mureş River and the basin of the two Târnava Rivers. The group of populations who entered into the intra-Carpathian area in the final phase of the first Iron Age (Hallstatt D or Ha.D) has been associated with Scythian-Iranian populations, mainly the Agathyrsi.[1]

Archaeological background

Belonging to the Scythian horizon in the intra-Carpathian area, the Sâncrai necropolis dates to 7th-5th centuries BC, a period that includes both the archaic phase and the final phase of this cultural group in Transylvania.

* Gabriel Balteş, PhD Candidate, Doctoral School of History, 1 Decembrie 1918 University of Alba Iulia, Romania; Archaeologist, The National Museum of Union, Alba Iulia; e-mail: gabi_baltes@yahoo.com. Mihai Gligor, PhD, Professor, Department of History, Archaeology and Museology, 1 Decembrie 1918 University of Alba Iulia, Romania; e-mail: mihai.gligor@uab.ro. Ioana D. Dulamă, PhD, Senior Researcher, Institute of Multidisciplinary Research for Science and Technology, Valahia University of Târgovişte, Romania; e-mail: dulama_id@yahoo.com. Cristiana Rădulescu, PhD, Professor, Faculty of Sciences and Arts, Valahia University of Târgovişte, Romania; e-mail: radulescucristiana@yahoo.com. Sofia Teodorescu, PhD, Scientific Researcher, Institute of Multidisciplinary Research for Science and Technology, Valahia University of Târgovişte, Romania; e-mail: sofiateodorescu@yahoo.com. Raluca M. Ştirbescu, PhD, Scientific Researcher, Institute of Multidisciplinary Research for Science and Technology, Valahia University of Târgovişte, Romania; e-mail: stirbescu_nic@yahoo.com. Ioan A. Bucurică, PhD, Scientific Researcher, Institute of Multidisciplinary Research for Science and Technology, Valahia University of Târgovişte, Romania; e-mail: bucurica_alin@yahoo.com. Sorina G. Stănescu, PhD, Scientific Researcher, Institute of Multidisciplinary Research for Science and Technology, Valahia University of Târgovişte, Romania; e-mail: geaninastanescu@yahoo.com.

[1] Valentin Vasiliev, *Sciții agatârși pe teritoriul României* [Scythian Agathyrsi on the Territory of Romania] (Cluj-Napoca: Dacia, 1980).

Annales Universitatis Apulensis Series Historica 25, I (2021): 37-56;
https://doi.org/10.29302/auash.2021.25.1.3.

Fig. 1. Google Maps capture showing the geographical location of Sâncrai necropolis (in red).

The necropolis is located in the middle basin of the Mureş River, in the interfluve between the Mureş and its tributaries, in a place called *Dâlma lui Candin/Darvas*. The necropolis sits on a high terrace, on the left bank of the Mureş River, in a position that provided good visibility towards the west-northwest,[2] where it is assumed settlements were located on the large terraces near the town of Aiud.[3]

The Iron Age necropolis was investigated in 2016, due to the development of the Sebeş-Turda Motorway (A10), a major road infrastructure project. The necropolis was excavated over a surface of 11.321 m² (Lot 2, km. 38 + 430 - 38 + 870). Two distinct necropolises were identified: one dating to the end of the first Iron Age (Ha.D), representing the Scythian horizon, and one dating to the middle of the second Iron Age (La Tène), representing the Celtic horizon.[4] Investigation of the Scythian necropolis led to the discovery of 95 burials, including both inhumation and cremation graves.[5] Study of the

[2] Ştefan Ferenczi, "Cimitirul scitic de la Ciumbrud (I)" [The Scythian Necropolis of Ciumbrud], *AMN* II (1965): 78-83.

[3] Alexandru Vulpe, "Descoperiri hallstattiene din zona Aiudului" [Discoveries Belonging to the Hallstatt Period from the Area of Aiud City], *Thraco-Dacica* V, 1-2 (1984): 55-56.

[4] Aurel Rustoiu, Gabriel Balteş, J. G. Nagy, "Sâncrai," *CCA* (2016): 210-211.

[5] Gabriel Balteş, "Din inventarul funerar al necropolei scitice de la Sâncrai (jud. Alba). Pumnale de tip akinakes" [The Funerary Inventory of the Scythian Necropolis of Sâncrai (Alba County). Akinakes Daggers], *BCŞS* 25 (2019): 5-23.

inhumation graves revealed a rich funerary inventory, mainly comprising ceramic vessels of different shapes and dimensions; weaponry including *akinakes* daggers, spear points, and arrowheads; jewellery pieces such as amber beads, kauri shells, kaolin, earrings, hair rings, *saltaleoni* bracelets, and clothing appliqués; and harness elements including horse bits and quiver appliqués.

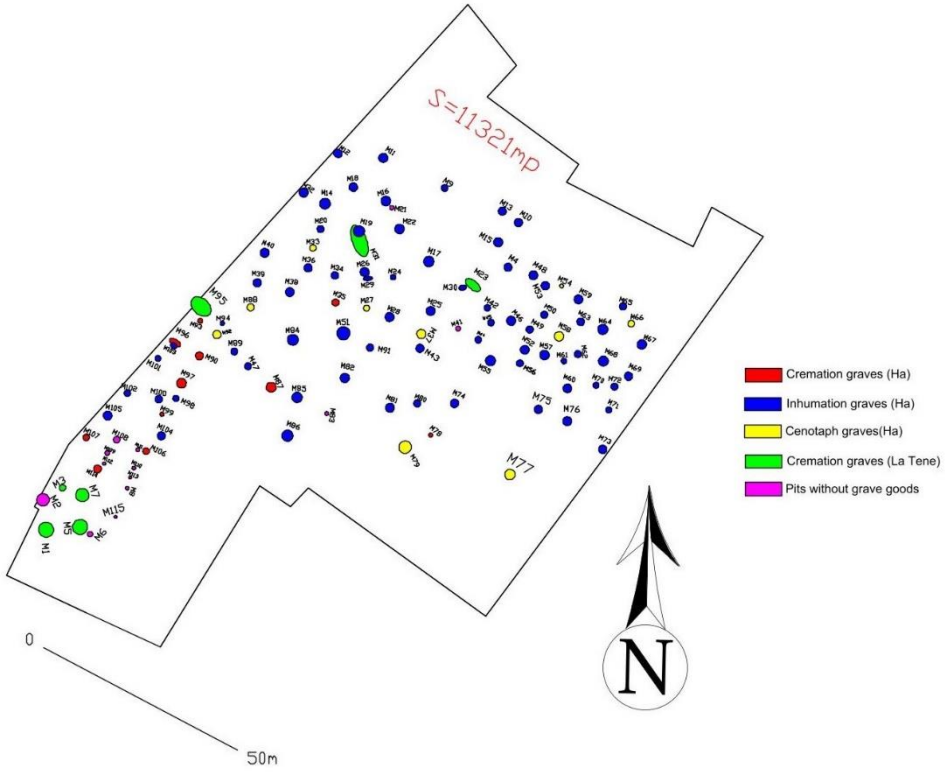

Fig. 2. Map with topographical distribution of excavated burials at Sâncrai necropolis.

Comprehensive interdisciplinary studies followed the excavation of the necropolis, for a thorough analysis of the recovered materials. Samples of the metallic artefacts were collected for archaeometric analysis. The purpose of this analysis was to examine the quality of the materials, the percentages of alloy elements, tool/weapon hardness, shape and arrangement of structural elements, fibre orientation in pieces made by plastic deformation (beating, die forging), the quality of welded joints, structural flaws (cracks, slag inclusions, etc.), ghosts (oxides, sulphites, etc.), and structural modifications triggered by thermic and thermochemical treatments or mechanical actions.[6] However, an even more

[6] Daniel Grolimund et al., "Shedding New Light on Historical Metal Samples Using Micro-Focused Synchrotron X-Ray Fluorescence and Spectroscopy," *Spectrochimica Acta* Part B, 59 (2004): 1627-1635.

important goal was gaining insight into the stages by which these processing techniques improved, as well as the ways in which various relationships or influences changed this process as a result of interactions between different populations.[7]

For the purpose of this analysis, 16 metallic samples with different features and uses were collected from inhumation graves (table 1; fig. 3).

Tab. 1. A10 – 10 Motorway Sebeș-Turda; S – Sâncrai; S.20 – Trench S.20; M – grave.

Code	Archaeologic Context	Description
S1	A10; S. 2016; S.20; M.60; inhumation grave	Axe. Dim.: 14cm, ⌀ 3 cm
S2	A10; S.2016; S.20; M.60; inhumation grave	*Akinakes* dagger. Dim.: 12 cm x 5 cm
S3	A10; S.2016; S.20; M.84; inhumation grave	*Akinakes* dagger. Dim.: 22 cm x 6 cm
S4	A10; S.2016; S.20; M.60; inhumation grave	Arrowhead. Dim.: 3,6 cm, ⌀ 2mm
S5	A10; S.2016; S.20; M.75; inhumation grave	Hair ring. Dim.: ⌀ 6,8 cm
S6	A10; S.2016; S.20; M.12; inhumation grave	Propeller shaped pendant. Dim.: ⌀ 4 cm
S7	A10; S.2016; S.20; M.12; inhumation grave	Saltaleoni bracelet. Dim.: 1.5, ⌀ 0,8 cm
S8	A10; S.2016; S.20; M.68; inhumation grave	Bead. Dim.: ⌀ 2 cm
S9	A10; S.2016; S.20; M.68; inhumation grave	Ring with 4 protuberances. Dim.: ⌀ 6 cm
S10	A10; S.2016; S.20; M.39; inhumation grave	Quiver appliqué. Dim.: 11 cm x 7 cm
S11	A10; S.2016; S.20; M.26; inhumation grave	Belt dispenser. Dim.: 3 cm x 3 cm
S12	A10; S.2016; S.20; M.26; inhumation grave	Horse-bit. Dim.: 17 cm x 2 cm
S13	A10; S.2016; S.20; M.75; inhumation grave	Clothing appliqué. Dim.: ⌀ 4 cm
S14	A10; S.2016; S.20; M.11; inhumation grave	Fibula. Dim: 5,5 cm x 3,5 cm
S15-S16	A10; S.2016; S.20; M.74; inhumation grave	Clothing appliqué (2 pieces). Dim.: ⌀ 2 cm

[7] Roxana Bugoi et al., "Archaeometallurgical Studies of Bronze Age Objects from the Romanian Cultural Heritage," *Rom. Rep. Phys.* 65, 4 (2013): 1234-1245.

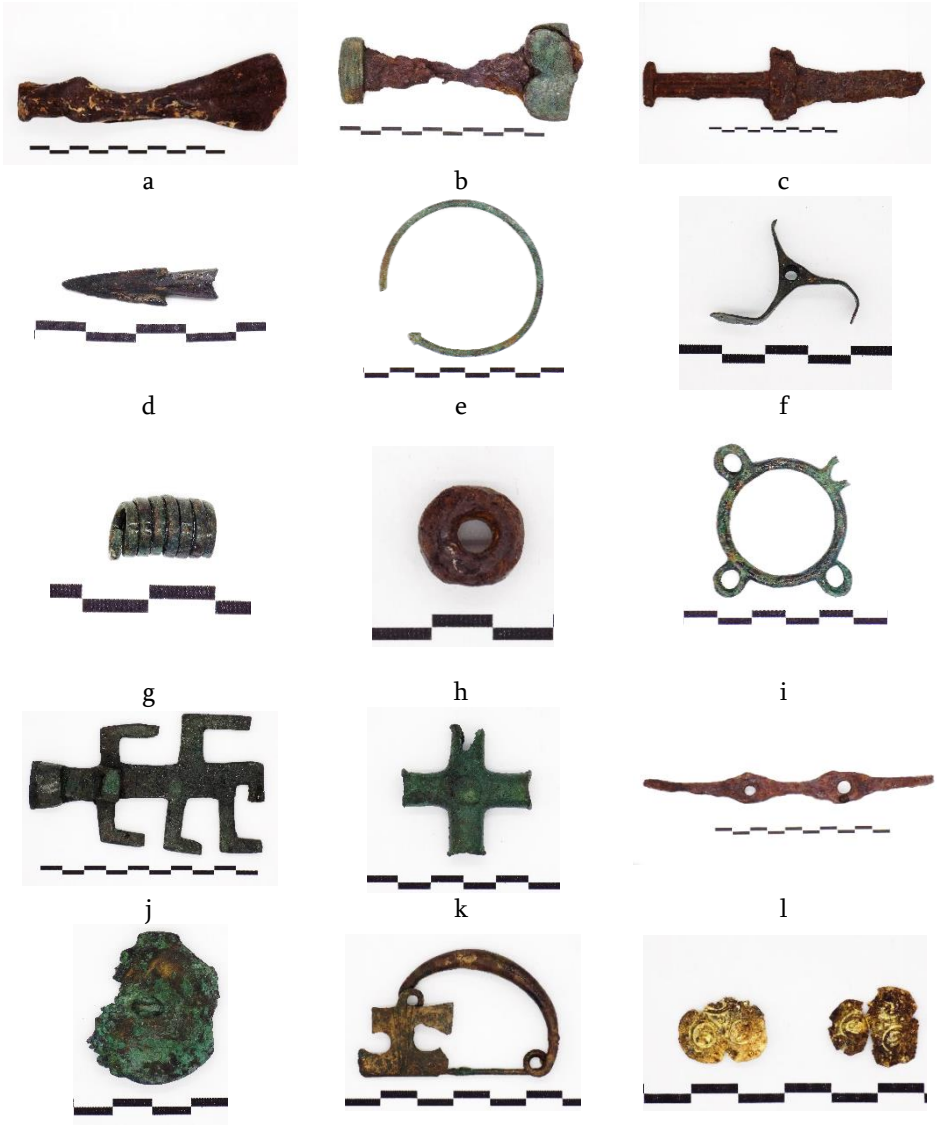

Fig. 3. Studied samples: a) axe (S1); b) *akinakes* dagger (S2); c) *akinakes* dagger (S3); d) arrowhead (S4); e) hair ring (S5); f) propeller-shaped pendant (S6); g) saltaleoni bracelet fragment (S7); h) bead (S8); i) ring with 4 protuberances (S9); j) quiver applique (S10); k) belt dispenser (S11); l) horse-bit (S12); m) clothing appliqué (S13); n) fibula (S14); o) clothing appliques, 2 pieces: S15 (left) and S16 (right).

Materials and methods

1) Optical Microscopy (OM)

The samples were visually analysed using Primo Star and Stemi 2000-c optical microscopes, equipped with an Axiocam 105 digital camera. The magnification varied from ×10 to ×100, depending on the size of the samples. Optical microscopy was used to examine the samples' visual characteristics and to compile preliminary reports regarding areas of interest to be studied further.[8]

2) Field Emission Scanning Electron Microscopy coupled with Energy Dispersive X-Ray Spectrometry (FE-SEM-EDS)

The next step in the analysis consisted of morphological investigations with an SU-70 microscope (Hitachi, Japan). This method allows for a more detailed analysis than MO, because the Field Emission microscope (FE-SEM) operates under high vacuum (10^{-8} Pa) and generates high resolution images (1 nm at 15 kV acceleration voltages). The SEM is coupled with an UltraDry detector (Thermo Fisher Scientific, USA) for energy dispersive X-ray spectrometry (EDS). The SEM images were obtained using 10 kV acceleration voltages at different working distances (17.6-18.7 mm), depending on sample characteristics. The advantage of the FE-SEM-EDS method lies in its versatility, as it not only allows a very accurate image to be obtained but also provides an elemental composition map. In this regard, the elemental content analysis was carried out at an acceleration voltage of 10 kV, using the Phi-Rho-Z correction method available in NSS software (Version 3.0).[9]

3) Attenuated Total Reflection – Fourier-Transform Infrared Spectroscopy (ATR-FTIR)

Fourier-transform infrared spectroscopy (FTIR) is mainly used to identify unknown compounds through molecular fingerprinting (it measures how much light is absorbed by the bonds of vibrating molecules), but it can also be used for estimating the presence of certain minerals in samples.[10] A VERTEX 80v spectrometer (Bruker, Ettlingen, Germany) was used for FTIR, equipped with an attenuated total reflection (ATR) sample stage and a Hyperion® microscope. The spectra were recorded in transmittance mode and obtained in the mid-infrared region of 3000-400 cm^{-1} (0.2 cm^{-1} spectral resolution and 0.1% T accuracy). Thirty-two scans were averaged to obtain clear transmittance spectra for each sample.[11]

---

[8] Ioan A. Bucurică et al., "Morphology and Physico-Chemical Characteristics of an Iron Fragment from Chaco Province," *Rom. J. Phys.* 64, 9-10 (2019): 4.

[9] Diana E. Tomuş (Szabo) et al., "Archaeometric Analyses on Precucuteni-Type Poterry from Transylvania (Romania). Case Study: Alba Iulia – *Lumea Nouă*," *J. Sci. Arts* 21, 1 (2021): 289.

[10] Chien-Pin Sherman Hsu, "Infrared Spectroscopy", in *Handbook of Instrumental Techniques for Analytical Chemistry*, ed. Frank A. Settle (New Jersey: Prentice Hall PTR, Upper Saddle River, 1997), 266.

[11] Alina Binţinţan et al., "Multielemental and Chemical Characterization of Eneolithic Petreşti Painted Pottery from the Alba Iulia-*Lumea Nouă* Archaeological Site, Romania," *Analytical*

4) Data Processing

Principal component analysis (PCA) was performed using IBM SPSS Statistics (Version 21) for cluster analysis as well as the Pearson's correlation analysis. The PCA and cluster analysis were used to evaluate the chemical similarities between metallic fragments,[12] while Pearson' correlations were applied to determinate the differences ($p < 0.05$) in elemental concentrations.

Results and discussion

Archaeometry is a growing field of research that uses techniques from the exact sciences (e.g., chemistry, physics, and mathematics) and natural sciences (e.g., geology and biology) with the purpose of adding more scientific value to results obtained by studies in the humanities (e.g., history, archaeology, anthropology).[13] This field of research also includes the application of analytical techniques and statistical methods in order to answer questions about the origin of materials,[14] dating,[15] prospecting, or reconstruction of a landscape.[16] In addition, the conservation and restoration of archaeological artefacts can also be considered part of the field of archaeometry.[17] The samples analysed in this study belong to the categories of weapons, ornaments, and harness parts.

Optical microscopy image show the presence of crystallised minerals on the surface of sample S1 (fig. 4a). These minerals may be associated with the material the axe was made from, because raw ores were used during the first Iron Age. However, they may also be associated with the soil matrix from which the metal was excavated. Longitudinal traces of abrasion can also be observed. These are caused by polishing or sharpening the axe on a hard surface (e.g., granite or natural sandstone). Sample S1 is characterised by a "snowflake" morphology, arranged in parallel layers[18] (fig. 4b).

Letters 52, 15 (2019): 2351.

[12] Alina Binţinţan et al., "Analysis and Structural Investigations on Early Eneolithic Foeni Painted Pottery from Alba Iulia-*Lumea Nouă* Archaeological Site," *Rom. J. Phys.* 64, 5-6 (2019): 11.

[13] Ioannis Liritzis et al., "Archaeometry: An Overview," *Scientific Culture* 6, 1 (2020): 51; L. Musílek, "Archaeometry – An Example of Interdisciplinarity in Engineering Education" (paper presented at the *43rd Annual SEFI Conference June 29 - July 2*, 2015, Orléans, France), 4; Peter Vandenabeele and Mary K. Donais, "Mobile Spectroscopic Instrumentation in Archaeometry Research," *Applied Spectroscopy* 70, 1 (2016): 27.

[14] Nikolaos Zacharias and Y. Bassiakos, "Dating of Artefacts", in *Nuclear Techniques for Cultural Heritage Research* [IAEA Radiation Technology Series No. 2] (Vienna: International Atomic Energy Agency, 2011), 86-89.

[15] Vandenabeele and Donais, "Mobile Spectroscopic Instrumentation," 27.

[16] Sofia Pescarin, *Reconstructing Ancient Landscape* (Budapest: Archaeolingua, 2009), 18.

[17] Antonio Doménech-Carbó, Maria Teresa Doménech-Carbó, and Virginia Costa, "Application of Instrumental Methods in the Analysis of Historic, Artistic and Archaeological Objects," in Antonio Doménech-Carbó, María Teresa Doménech-Carbó, and Virginia Costa, eds., *Electrochemical Methods in Archaeometry, Conservation and Restoration. Monographs in Electrochemistry* (Berlin, Heidelberg: Springer, 2009), 1-2.

[18] David A. Scott, *Metallography and Microstructure of Ancient and Historic Metals* (Singapore: Tien Wah Press, 1991), 42.

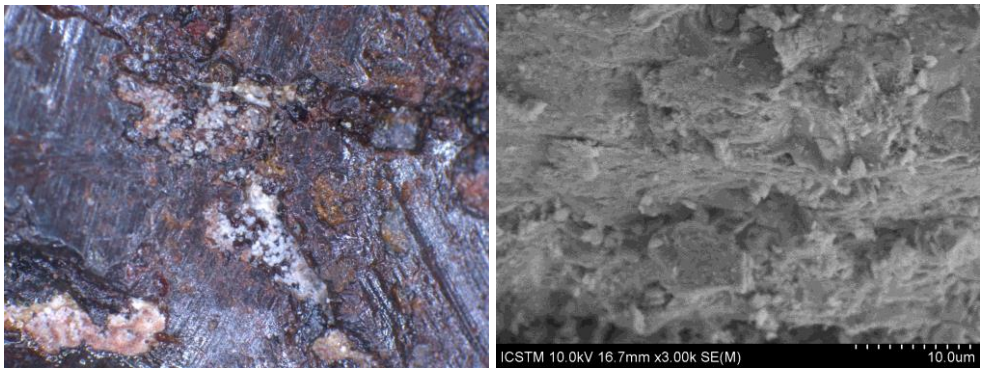

Fig. 4. Sample S1: a) Optical microscopy image (10X); b) SEM image (3 kX).

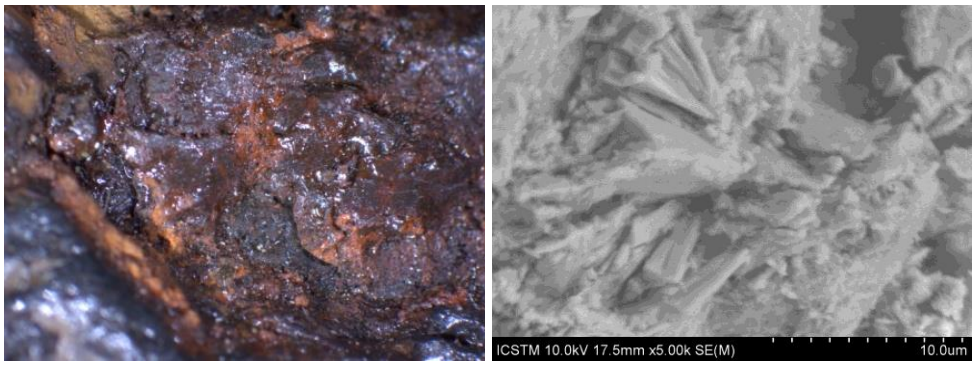

Fig. 5. Sample S2: a) Optical microscopy image (10X); b) SEM image (5 kX).

The images obtained from sample S2 do not show crystallised minerals like those observed on the surface of sample S1 (fig. 5a). Even though the sample was coated with resin, a scale structure can be observed, most likely caused by repeated hitting with a flat-ended object. Sample S2 is characterised by acicular structures with a disordered arrangement, and the green areas do not differ in terms of structure[19] (fig. 5b).

The optical microscopy images for sample S3 (fig. 6a) highlighted two aspects: a scale structure similar to the one observed in the S2 sample, as well as small inclusions of crystallised minerals. The electron microscopy images (fig. 6b-d) reveal that sample S3 consists of several completely different types of structures: a perfectly flat, lamellar structure, associated with pearlite (fig. 6b),[20] a disordered, aerated structure composed of thin slats (<1 μm) (fig. 6c), and a disordered compact structure composed of thin slats (<0.5 μm) specific to iron

[19] Ibid., 27.
[20] Ibid., 13.

oxide nanoblades[21] (fig. 6d).

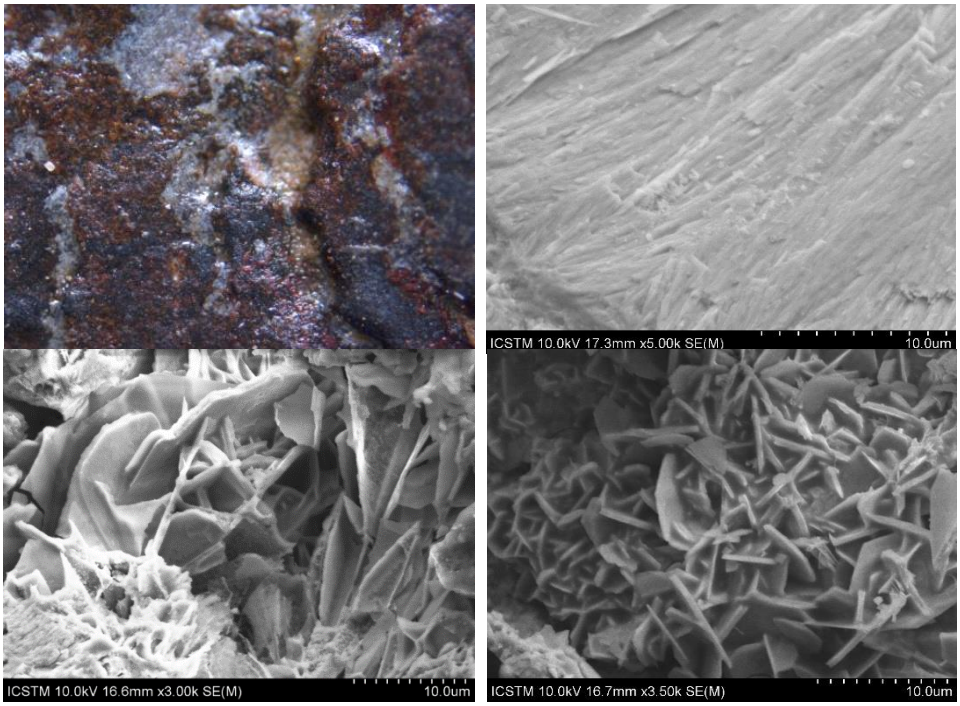

Fig. 6. Sample S3: a) Optical microscopy image (40X); b) SEM image (5 kX); c) SEM image (3 kX,, d) SEM image (3.5 kX).

Longitudinal traces of abrasion caused by an attempt to polish or sharpen the arrowhead on a hard surface (e.g., granite or natural sandstone) were revealed in the OM images (fig. 7a) of sample S4. In addition, the granular structure[22] of the metal in the area where the oxide layer was missing or was exfoliated was closely observed. The microstructure of sample S4 is a compact coarse ("rocky") structure with lamellar inclusions[23] (fig. 7b).

[21] Wenhui Zhu et al., "In Situ Atomic-Scale Probing of the Reduction Dynamics of Two-Dimensional Fe_2O_3 Nanostructures," in *ACS Nano* 11, 1 (2017): 645-664, fig. 1.
[22] Scott, *Metallography*, xvi.
[23] Ibid.

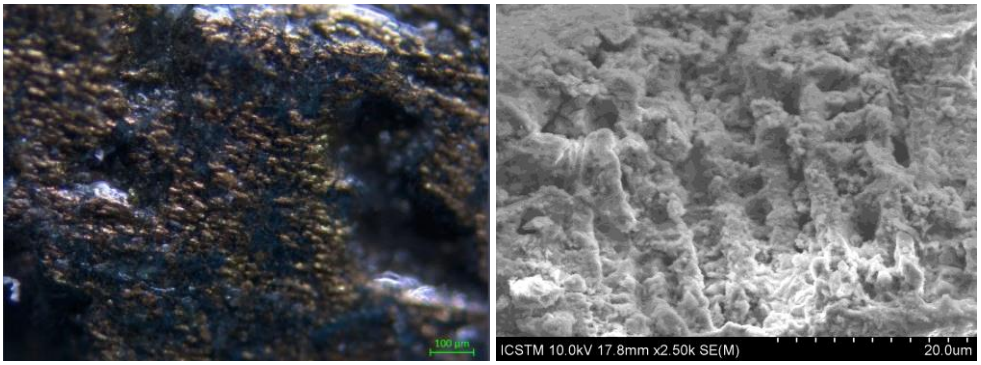

Fig. 7. Sample S4: a) Optical microscopy image (100X); b) SEM image (2.5 kX).

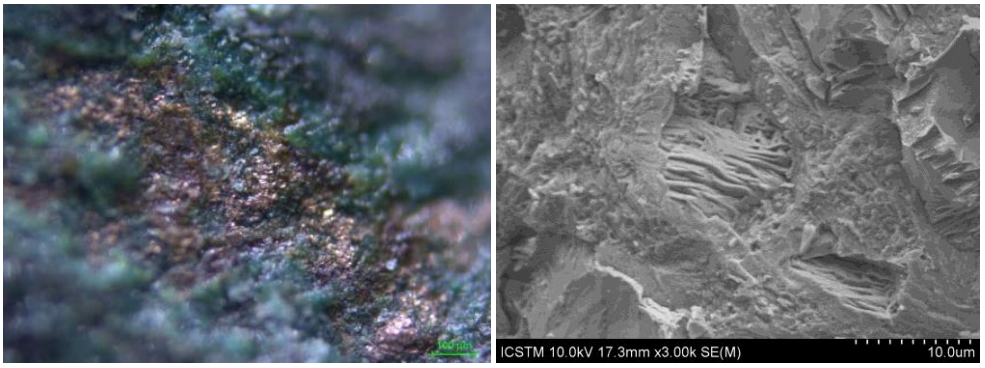

Fig. 8. Sample S5: a) Optical microscopy image (40X); b) SEM image (3 kX).

Optical microscopy images of sample S5 show the granular structure of the metal in the area where the oxide layer was missing or exfoliated. The "perfect" shape of the metal part was caused by grinding on hard but fine materials (e.g., granite, hone, or other natural sandstone). No traces of grinding were found (fig. 8a). Sample S5 is characterised by a lamellar/acicular structure with dendritic and porous inclusions[24] (fig. 8b).

Optical microscopy images of sample S6 show (fig. 9a) the scale structure most likely caused by repeated shots (observed in other samples and described above – S2 and S3). It also reveals fine crystalline inclusions, most likely caused by the soil in which samples were conserved. Sample S6 is characterised by a lamellar structure, with parallel layers and small disordered granular inclusions[25] (fig. 9b).

[24] Ibid., xviii.
[25] Ibid., 29.

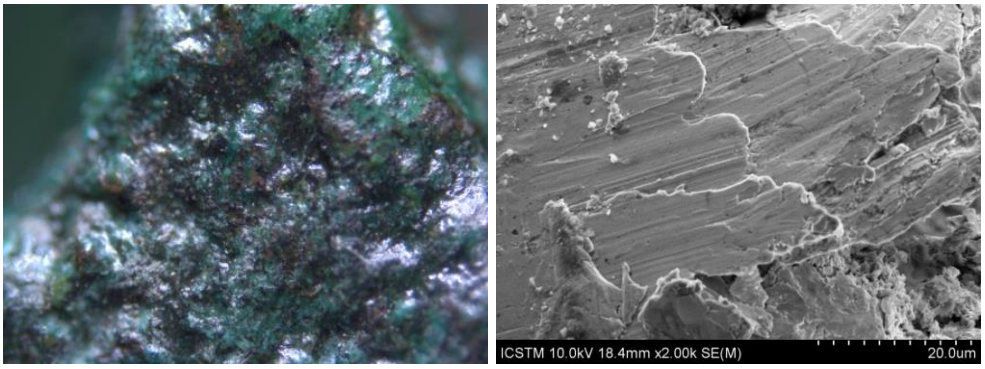

Fig. 9. Sample S6: a) Optical microscopy image (40X); b) SEM image (2 kX).

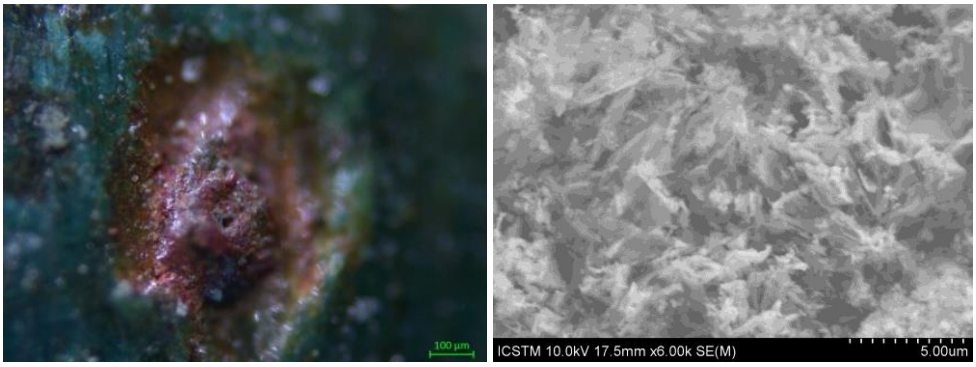

Fig. 10. Sample S7: a) Optical microscopy image (100X); b) SEM image (6 kX).

Fine abrasion marks were observed through optical microscopy on sample S7. The granular structure of the metal in the area where the outer layer was missing or exfoliated was closely observed (fig. 10a). Similar to sample S6, sample S7 has fine crystalline inclusions on its surface. Sample S7 is characterised by a disordered dendritic "snowflake" morphology[26] (fig. 10b).

The presence of crystallised structures on the surface of sample S8 can be observed (fig. 11a). Similar to the structures seen in sample S1, these may derive either from the base material from which the bead was made or from the soil from which it was excavated. Traces of abrasion resulting from polishing or perforating the material can also be observed (fig. 11b). Sample S8 is characterised by a compact, coarse ("rocky") morphology with multiple microcracks.[27]

[26] Ibid., 140.
[27] Ibid., 102.

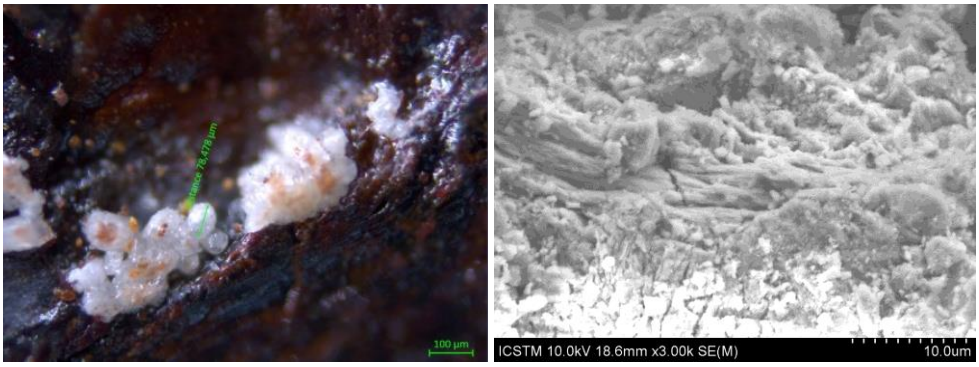

Fig. 11. Sample S8: a) Optical microscopy image (100X); b) SEM image (3 kX).

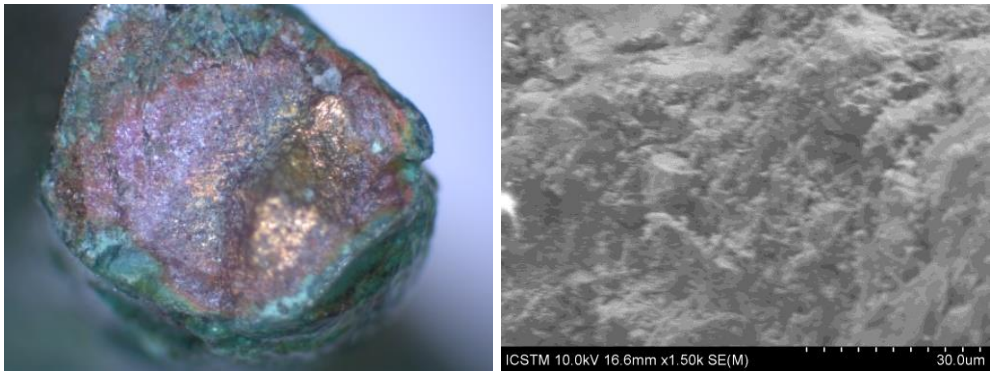

Fig. 12. Sample S9: a) Optical microscopy image (40X); b) SEM image (1.5 kX).

Sample S9 shows traces of repeated impacts with a flat-ended object, but no abrasion marks can be observed (fig. 12a). The morphology can be described as compact and porous[28] (fig. 12b).

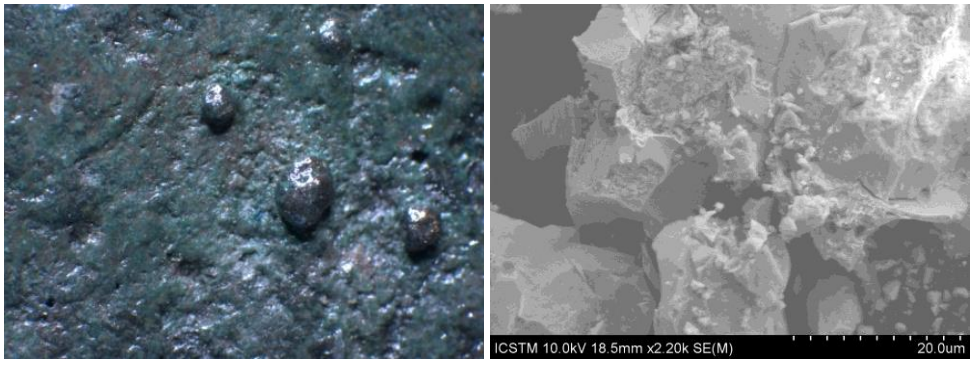

Fig. 13. Sample S10: a) Optical microscopy image (10X); b) SEM image (2.2 kX).

[28] Ibid., 104.

Sample S10 shows a scale structure, most likely caused by repeated hitting with a flat-ended object. In addition, "drops" were observed on the surface of this sample; these appear to be molten metal (fig. 13a). Sample S10 is characterised by a compact and coarse morphology with serious intergranular cracks[29] (fig. 13b).

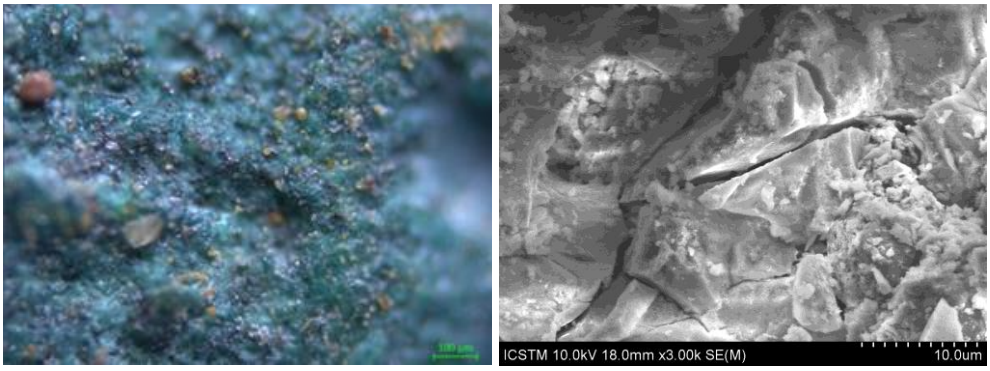

Fig. 14. Sample S11: a) Optical microscopy image (100X); b) SEM image (3 kX).

The presence of minerals on the surface of sample S11 can be observed in the optical microscopy images (fig. 14a). Traces of processing can also be seen, likely caused by repeated hitting with a sharp-tipped or small object. In terms of morphology, sample S11 is compact, with concentric microcracks and microlayers (probably caused by the inclusions present in the copper mass)[30] (fig. 14b).

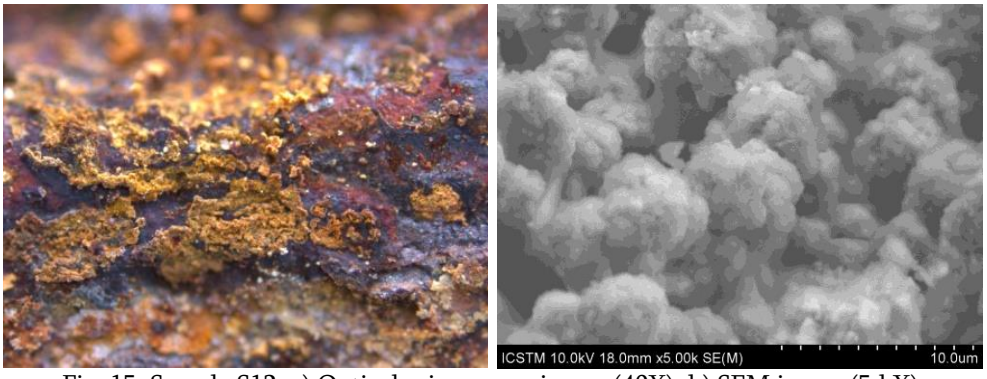

Fig. 15. Sample S12: a) Optical microscopy image (40X); b) SEM image (5 kX).

The optical microscopy images show that sample S12 has a scale structure, most likely caused by repeated hitting with a flat-ended object. In

[29] Ibid., 120.
[30] Ibid., 103.

addition, the granular/reticular structure of the oxide layer at the sample surface was closely observed. The SEM images obtained for sample S12 show the granular morphology, globules with dendritic distribution.[31]

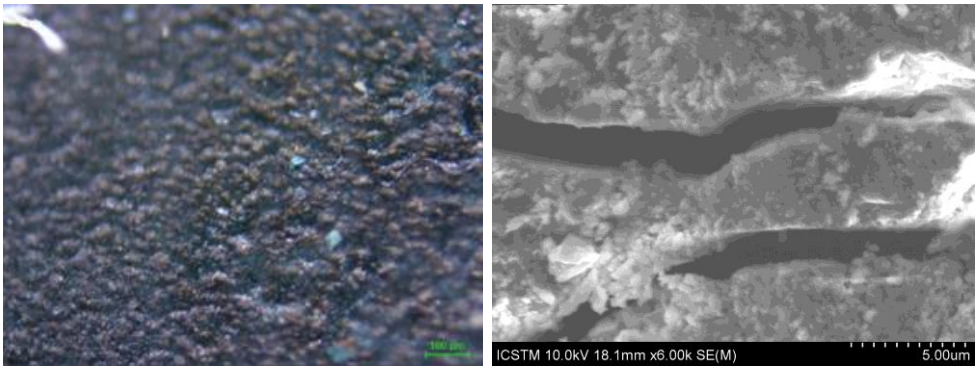

Fig. 16. Sample S13: a) Optical microscopy image (100X); b) SEM image (6 kX).

Optical microscopy investigations on sample S13 showed a granular structure (fig. 16a). The "perfect" surface was likely caused by grinding on hard but fine materials, because discrete traces of grinding can be observed with some difficulty. Sample S13 is characterised by a compact morphology with small granular inclusions and coarse cracks (fig. 16b).

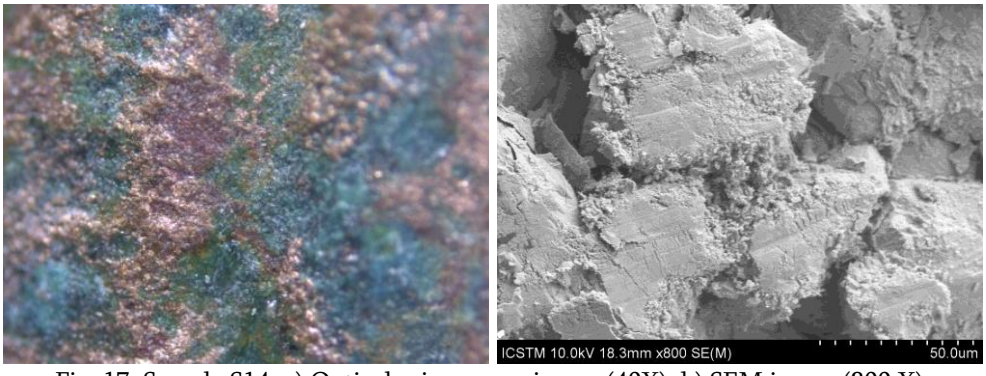

Fig. 17. Sample S14: a) Optical microscopy image (40X); b) SEM image (800 X).

Figure 17a highlights sample S14's scale structure, most likely caused by repeated blows (observed in other tests described above), but also the precise technique used in manufacturing and decorating the piece. In addition, fine crystalline inclusions, most likely from the soil (fig. 17b), can be observed in this sample. Sample S14 is characterised by a perfectly flat, lamellar structure with fine granular inclusions.

[31] Ibid., 5.

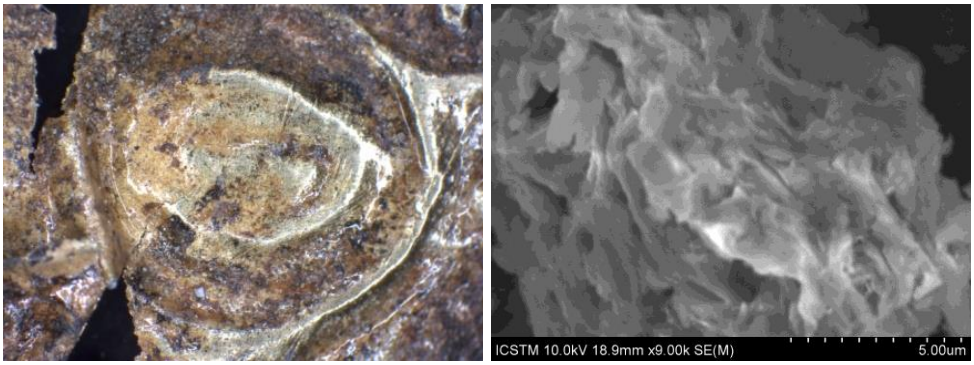

Fig. 18. Sample S15: a) Optical microscopy image (10X); b) SEM image (9 kX).

Samples S15 and S16 were created by fine engraving with circular-concentric shapes on thin metal sheets, obtained by grinding. Small-pointed objects with a small diameter were used to create the shapes (fig. 18a and 19a). These samples are characterised by a "snowflake" morphology and elongated lamellar regions[32] (fig. 18b and 19b).

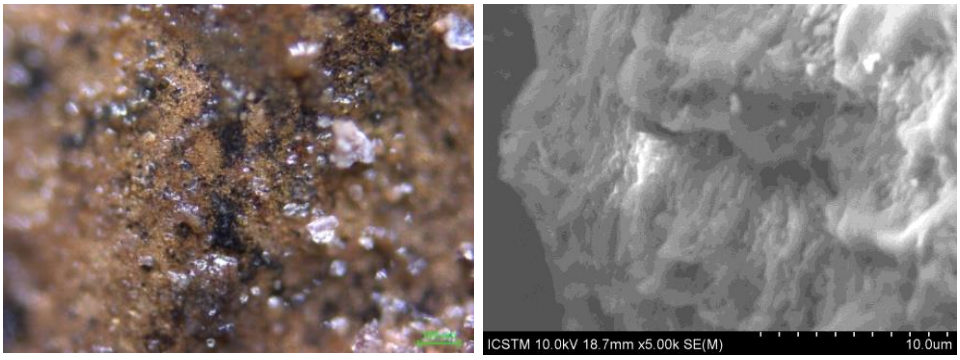

Fig. 19. Sample S16: a) Optical microscopy image (100X); b) SEM image (5 kX).

The EDS results for all analysed sample are presented in tab. 2. Carbon, oxygen, and aluminium were recorded in each sample, but their values vary between samples. These elements are usually present in minerals as well as in clay soils.[33]

[32] Ibid., 91.
[33] Alina Binţinţan et al., "ATR-FTIR and SEM-EDS Analyses of Lumea Noua Painted Pottery from Alba Iulia-Lumea Nouă Neolithic Site," in *Rev. de Chim.* 68, 4 (2017): 850, tab. 5.

Tab. 2. Elemental content of samples, obtained by EDS analysis and expressed in wt.%.

wt.%	S1	S2	S3	S4	S5	S6	S7	S8	S9	S10	S11	S12	S13	S14	S15	S16
C	4.05	10.19	6.87	2.47	2.69	3.35	9.43	4.85	16.22	3.26	5.82	11.00	14.08	10.31	1.24	1.9
N													1.91		0.57	
O	30.73	34.74	31.2	11.85	23.38	4.75	9.76	36.47	22.72	22.41	24.09	34.76	43.16	9.06	1.1	6.2
F													3.41			
Na	1.58							1.57								
Mg		0.25							0.4	0.11	0.19		0.64			
Al	0.37	1.51	1.23	0.26	0.33	1.29	0.67	0.29	0.93	0.37	0.49	2.75	5.62	8.26	0.38	1.73
Si	0.45	3.21			1.99	1.41		1.43		2.24	0.62		10.38			3.93
P		0.5						1.7	0.54	0.52	2.81					
S		0.17						0.81				3.31				
K		0.23														
Ca	0.94	0.73				0.25		8.31					1.1			10.82
Cl			0.69	1.82	0.22		0.22									
Fe	61.87	46.99	60.02					44.56				42.79				
Co				0.12		0.59	0.33									
Sc									0.07		0.08					
Cu		1.47		77.07	55.28	81.08	65.61		19.65	21.04	28.47		5.14	11.32	1.81	
Mo						0.27										
As					0.47											
Sn				6.42	15.64	5.5	13.98		39.47	45.72	35.76	5.38	13.54	61.04		
Ag															28.09	27.51
Au															64.54	47.93
Pb						1.53				4.34	1.57				2.27	
Ir													1.03			

Based on the EDS data, principal component analysis and cluster analysis were carried out. As can be observed in fig. 18-19, the analysed samples are arranged in 3 clusters:

- The first group of samples (S1, S2, S3, S8, and S12) is characterised by a high iron content (42.79-60.02 wt.%), with an average value of 50.04 wt.%; these samples also contain elements such as Na (S1, S8), Si, and Ca (S1, S2, and S8).
- The second group of samples (S4, S5, S6, S7, S9, S10, S11, S13, and S14) is characterised by a high copper content (5.14-81.08 wt.%, with an average value of 40.52 wt.%) as well as the presence of tin (5.50-61.04 wt.%, with an average value of 26.34 wt.%). The samples in this group also contain Si (S5, S6, S10, S11, and S13), P (S9, S10, and S11), Ca (S6 and S13), Cl (S4, S5, and S7), Co (S4, S6, and S7), Sc (S9 and S11), Mo (S6), As (S5), Pb (S6, S10, and S11), and Ir (S13).
- The third group of samples (S15 and S16) is characterised by a high gold content (47.93-64.54 wt.%, with an average value of 56.24 wt.%) along with silver (27.51-28.09 wt.%, with an average value of 27.80 wt.%).

The values recorded for Si and Ca, correlated with infrared data (tab. 4), show traces of soil/clay. In addition, the high Ca content in samples S8 and S16 can be explained by the presence of $CaCO_3$ (calcite) or $CaSO_4$ (gypsum).

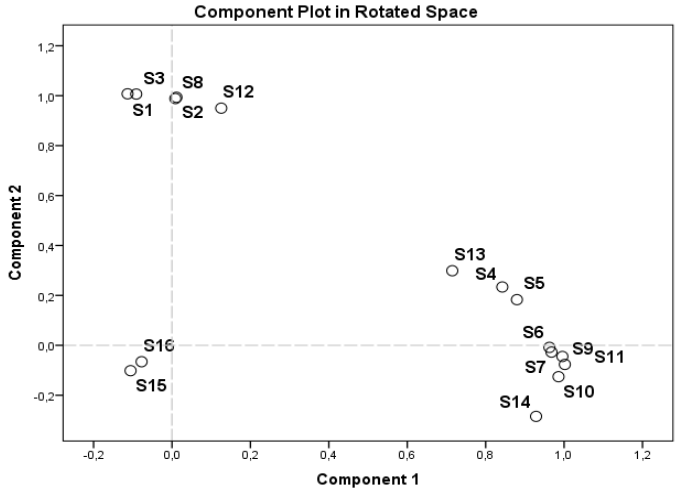

Fig. 20. Principal component analysis.

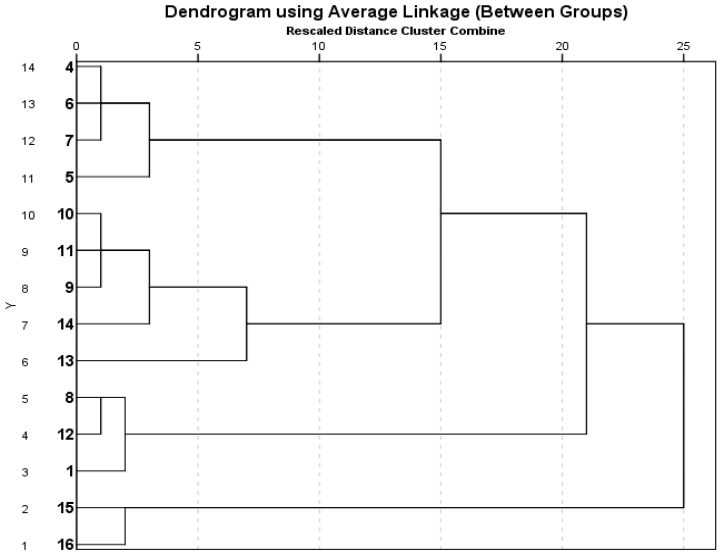

Fig. 21. Cluster analysis.

In fig. 21, samples S2 and S3 are not visible in the cluster because they are similar to S8 and S1, respectively.

In order to evaluate the similarities between samples, the Pearson's correlations matrix was used, based on the EDS data (tab. 3). This method allows highlighting of samples with similar chemical content ($p>0.5$). These values are marked with bold font in tab. 3.

Tab. 3. Pearson' correlations matrix of elemental content.

S1	S2	S3	S4	S5	S6	S7	S8	S9	S10	S11	S12	S13	S14	S15	S16	
1.000	**0.975**	**0.998**	0.326	0.300	0.154	0.154	**0.964**	0.134	0.108	0.163	**0.957**	0.327	-0.020	-0.092	-0.070	**S1**
	1.000	**0.983**	0.476	0.436	0.296	0.282	**0.983**	0.237	0.173	0.255	**0.990**	0.508	0.011	-0.104	-0.065	**S2**
		1.000	0.349	0.317	0.183	0.185	**0.965**	0.157	0.117	0.178	**0.967**	0.354	-0.009	-0.092	-0.071	**S3**
			1.000	**0.988**	**0.861**	**0.838**	0.494	**0.830**	**0.784**	**0.871**	**0.557**	**0.941**	**0.567**	-0.090	-0.026	**S4**
				1.000	**0.870**	**0.835**	0.459	**0.853**	**0.845**	**0.912**	**0.518**	**0.914**	**0.633**	-0.094	-0.031	**S5**
					1.000	**0.950**	0.269	**0.935**	**0.873**	**0.907**	0.386	0.813	**0.784**	-0.144	-0.103	**S6**
						1.000	0.251	**0.981**	**0.875**	**0.919**	0.384	0.743	0.833	-0.107	-0.079	**S7**
							1.000	0.221	0.182	0.264	**0.972**	**0.509**	-0.006	-0.109	-0.043	**S8**
								1.000	**0.950**	**0.970**	0.345	**0.695**	**0.906**	-0.103	-0.081	**S9**
									1.000	**0.984**	0.277	**0.609**	**0.930**	-0.096	-0.080	**S10**
										1.000	0.359	**0.716**	**0.884**	-0.102	-0.075	**S11**
											1.000	**0.560**	0.119	-0.111	-0.077	**S12**
												1.000	0.382	-0.118	-0.032	**S13**
													1.000	-0.091	-0.099	**S14**
														1.000	**0.968**	**S15**
															1.000	**S16**

Tab. 4. Characteristic bands of wavenumbers in the mid-infrared region (4000-600 cm^{-1}) and far-infrared region (600-230 cm^{-1}).

Wave-numbers [cm^{-1}]	Assignments	S1	S2	S3	S4	S5	S6	S7	S8	S9	S10	S11	S12	S13	S14	S15	S16
360-370 410-420	**FeOOH**	X X	 X	X X					X				X X				
385-400	**Fe_2O_3**	X	X	X					XX				XX				
435 520	**Fe-O**	X X	X	 X					X				X				
495-500	**$CaSO_4$**				X			X			X	X		X	X	X	X
441-450 665-670	**Cu-O**				X X	X X	X X	X X		X X	X X	X X		X X	X X	X X	
670-700	**$FeCl_2$**		X	X									X				
710-715	**CO_3^{2-}**			X			X										
455-465 740-750 780-800	**Si-O (quartz)**	X X	X XX	X X XX	X X	X X	X X	 X X	 X	 X	 X X	 X X	 X	 X	 X	X X X	X X X
1000-1140	**Si-O (clay minerals)**	XX	X	XX	XX	X	XX	X	X	XX		XX	X	XX	XX		
460-530	**Au-Ag**															X	X

The purpose of using the FTIR method was to obtain spectral signatures for metallic samples. All samples present oxides on the surface as a result of interaction between the samples and the soil. Soil parameters such as pH and humidity play an important role in the conservation of archaeological samples.

The spectral data obtained from the studied samples are presented in tab. 4. All samples show spectral data associated with an Si-O bond from quartz or clay minerals, but only half of the samples reveal the presence of gypsum ($CaSO_4$). In samples S1, S2, S3, S8, and S12, iron-based minerals such as goethite (FeOOH), ferric oxide (Fe_2O_3), and ferrous chloride ($FeCl_2$) were identified.[34]

Metals do not absorb infrared light because the vibrational frequencies of the metal-metal bonds are beyond the range of conventional FTIR spectrometers (700-6000 cm^{-1}). For a qualitative investigation of functional metallic groups, particularly metal-metal bonds, the infrared absorption band was observed for each vibrational degree of freedom when a change occurred in the dipole moment during vibration. In this regard, the samples in the copper-based group were assigned the spectral data (tab. 4) characteristic of a Cu-O bond,[35] for example cupric oxide (CuO) or cuprous oxide (Cu_2O). The spectral features specific to Ag-Au bonds (tab. 4), as well as an understanding of the interactions of these metallic samples with climatic and other factors was crucial to the assignment on the far-infrared region (below 600 cm^{-1})[36] for samples S15 and S16.

Conclusions

A combination of non-invasive/micro-destructive analytical techniques (SEM-EDS and FTIR) and statistical methods (cluster analysis, using SPSS Statistics) was used to obtain comprehensive information about the studied metal artefacts. Overall, the analytical and statistical analyses show us that metallic samples can be grouped into three clusters based on content: iron (S1, S2, S3, S8, and S12), gold-silver (S15 and S16) and copper-tin alloy. The last cluster can be divided into 2 classes: one with Cu as a major constituent (S4, S5, S6, and S7), the other with Sn as a major constituent (S9, S10, S11, S13, and S14). According to scientific literature, the Cu-Sn alloy with 12-22 wt.% content of tin is considered bronze[37] (S5, S7, and S13). Within all these groups, samples present a

[34] Almir Olovčić et al., "Chemical Analysis of Iron Slags and Metallic Artefacts from Early Iron Age," *International Research Journal of Pure & Applied Chemistry* 4, 6 (2014): 868.

[35] Wugan Luo et al., "Tentative Determination of a Special Bronze Material by Multiple Technological Test on a Xuan-Liu Dagger-Axe from the Xujialing Site, the Eastern Zhou Period, Henan Province, China," *J. Cult. Herit.* 46 (2020): 308, tab. 4.

[36] Olga B. Belskaya et al., "FTIR Spectroscopy of Adsorbed Probe Molecules for Analyzing the Surface Properties of Supported Pt(Pd) Catalysts," in Theophanides Theophile, ed., *Infrared Spectroscopy – Materials Science, Engineering and Technology* (Rijeka: Intech, 2012), 149-172.

[37] Marta Quaranta et al., "Chinese Archaeological Artefacts: Microstructure and Corrosion Behaviour of High-Leaded Bronzes," *J. Cult. Herit.* 15, 3 (2014): 283-291.

strong correlation, supporting the hypothesis that they were obtained using the same or similar minerals.

Regarding manufacturing technology, even though the thin sections of these samples have not yet been studied, the regular structures characteristic of melting samples can clearly be observed (S2, S3, S4, S5, S6, S10, S11, and S13). In addition, it is clear from the data presented here that samples S15 and S16 were created through successive heating and beating processes.

Acknowledgement

This work was supported by Gabriel Balteş doctoral grant and by the project UEFISCDI - 51PCCDI/2018, "New diagnosis and treatment technologies for the preservation and revitalization of archaeological components of the national cultural heritage".